Mem. S.A.It. Suppl. Vol. 9, 59

Memorie della
Supplementi

High-resolution IBIS Observations and Comparison with 3D Simulations

A. Asensio Ramos*, K. Janssen*, G. Cauzzi and K. Reardon

Istituto Nazionale di Astrofisica – Osservatorio Astrofisico di Arcetri, Largo E. Fermi, I-50125 Firenze, Italy
e-mail: aasensio@arcetri.astro.it
* ESMN Fellow

Abstract. High resolution observations of a very quiet region of the solar surface have been obtained with IBIS (Interferometric BIdimensional Spectrometer) in the non-magnetic Fe I 7090.4 Å spectral line. We present a first comparison between the observed, spatially resolved, spectral data and the simulated spectra in a 3D snapshot of a radiation-hydrodynamical simulation of the solar atmosphere. Preliminary results indicate that the simulations reproduce quite well many of the observational properties of the high resolution IBIS data, even though the simulations present a velocity distribution that contains values quite larger than the observed ones.

Key words. Sun: photosphere – Sun: granulation – Sun: radiation-hydrodynamical simulations

1. Introduction

It is of interest to compare the recent three-dimensional radiation hydrodynamical simulations of the solar atmosphere with high-resolution observations. Until now, the majority of such comparisons have focused on the spatially averaged spectral profile emerging from the simulations and the revision of atomic abundances in the solar atmosphere (Asplund et al. 2000,and following papers). The high spatial and spectral resolution reached by the new IBIS instrument installed at the Dunn Solar Telescope of NSO (Cavallini & Reardon, this volume), allow a direct comparison of the point-to-point properties of the emergent profiles and the physical information we can obtain from them.

2. Observations

The observations for this contribution were obtained with the Interferometric BIdimensional Spectrometer (IBIS) on June 2nd, 2004, employing the high order Adaptive Optics system. IBIS is based on two Fabry Perot Interferometers mounted in collimated configuration, and provides narrowband (20–40 mÅ FWHM), two-dimensional images of the solar surface, 80" in diameter. The system is rapidly tunable in wavelength, so the spectral scan of a typical photospheric line can be accomplished in a few seconds. We show here data obtained in the photospheric non-magnetic FeI 7090.4 Å line in a very quiet region at disk cen-

Send offprint requests to: A. Asensio Ramos

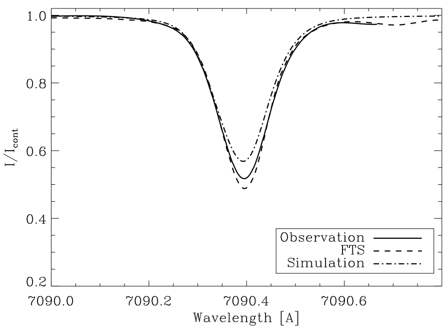

Fig. 1. Spatial and temporal average of the FeI 7090 Å spectral line observed with IBIS (solid black line) compared with the FTS disk-center intensity atlas (dashed line) and with the synthetic line averaged over the 50×50 points in the horizontal direction on the 3D snapshot (dashed-dotted line). The difference between the atlas and the observed profile is produced by the smaller spectral resolution of IBIS. The differences between the synthetic and observed profiles are probably related to the fact that the average for the synthetic case is only done in one snapshot.

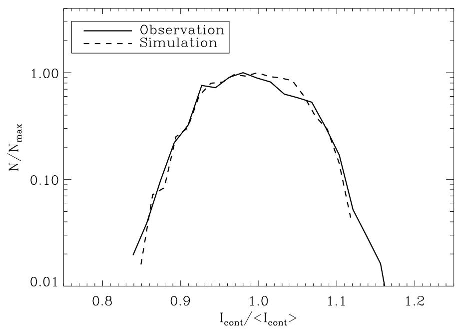

Fig. 2. Brightness distribution in the continuum for the observed data (solid) and the simulations (dashed), after convolving the monochromatic images with the telescope and atmospheric PSFs. The importance of the atmosphere has been varied until obtaining a synthetic contrast equal to the observed one. It is important to note that, after fitting the observed contrast, the whole distribution is immediately fitted.

ter. Pixelsize was 0.17" × 0.17", and the line was sampled in 16 wavelength positions (mean stepsize 30 mÅ). A cutout of 50 × 50 pixels (the same size as the simulations, see below) was chosen from a representative scan out of the one hour time series. After the dark current subtraction and division by the 3D gain table, 16 monochromatic images are created by removing the effect of instrumental blueshift over the field of view.

3. Synthetic spectrum

The synthetic spectral lines were obtained by solving the radiative transfer (RT) equation for vertical incidence in a three-dimensional snapshot of the radiation-hydrodynamical simulation of the solar atmosphere of Asplund et al. (2000). We have assumed that the line is formed in Local Thermodynamical Equilibrium. The RT equation is solved using the parabolic version of the short-characteristics method (Olson, Auer, & Buchler 1986).

The snapshot consists of a cube of 50x50x102 points in which the temperature, hydrogen and electron density and velocity vector are known. The horizontal size of the simulation box is 6 Mm, with a step size of 120 km per grid point (the same as the observations). The vertical direction extends from −200 km to 800 km. This constitutes only the part of the whole simulation box which is associated with the photospheric region where the lines are being formed. Once the emergent spectrum is obtained for each of the 50x50 points in the surface, we performed the horizontal average to compare with the atlas. Figure 1 presents the comparison between the average line profile obtained from the IBIS observations and from the synthesis in the 3D snapshot, together with the FTS disk-center intensity atlas by Brault & Neckel (1987). The difference between the observed and the synthetic profiles is of the order of 10 %.

4. Comparison

In order to perform meaningful comparisons, we have degraded the simulated images to the actual spatial and spectral resolution of the observed data. In particular, we included the PSF

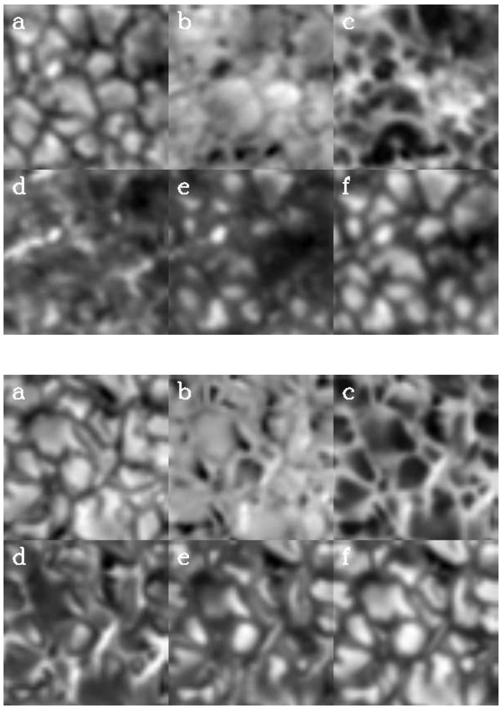

Fig. 3. Observed (upper panel) and synthetic (lower panel) monochromatic images at different wavelength positions through the FeI 7090 Å spectral line. Image (a) is in the continuum, (d) is in the core of the line, (b-c) are in the blue wing, while (e-f) are in the red wing.

of the telescope and the PSF of the atmosphere. The atmosphere contribution is varied until the contrast over the whole image is equal in both the observations and the simulations, as described in Collados & Vázquez (1987). Figure 2 shows the brightness distribution in the continuum $I_{\mathrm{cont}}/\langle I_{\mathrm{cont}}\rangle$. Taking into account that we have fitted only one parameter, the simulations are able to reproduce very nicely the whole observed brightness distribution.

Figure 3 presents monochromatic images at different wavelength positions through the line. The upper panel presents the observed data while the lower panel presents the synthetic data, degraded as explained above. Obviously they do not represent the same region in the solar surface, but this comparison helps us evaluate the ability of the simulations to reproduce the morphological properties of the observed convection. Image *a* is taken at the continuum close to 7090 Å while image *d* is taken at the core of the line. Images *b-c* and *e-f* are taken in the blue and red wing of the line, respectively (±30, ±60 mÅ). The intensity pattern in the wings of the line is very different from blue to red, an effect well reproduced by the simulations. In the blue wing, closest to the core, we see a pattern quite reminiscent of an "inverted granulation", while in the red wing, especially further out in the line, we only see "standard granulation", but enhanced with respect to the continuum. This is produced by the important cross-talk between the velocity and the intensity. In fact, at any fixed wavelength in the blue wing, in the red-shifted integranular lanes we see radiation coming from closer to the continuum, while in the blue-shifted granular material we see closer to the core of the line. As a consequence, the intensity of the radiation coming from the granules is smaller than that coming from the intergranules and we see the inverted granulation. The reverse holds in the red wing, and since the intensity in the granules is larger than in the intergranules, we see an enhanced granulation. Further, it must be kept in mind that also the "real" inverted granulation produced by the inversion of the temperature trend with height (granules become cooler than intergranules above ~200-250 km) is mixed with the velocity effects. Indeed, if we artificially align all the lines to have the same velocity, this real inverted granulation is observed in the core of the line both in the observation and in the simulation.

These same properties are presented in a more quantitative way in Figure 4, where we plot the correlation between the intensity at each sampled wavelength vs. the intensity in the continuum (thick lines), for both observations and simulations. The dotted line is the observed average line profile. Anticorrelation with the continuum image (inverted granulation) is always in the blue wing of the line, being the correlation at the core very close to zero. This demostrates the morphological properties discussed above. If we artificially set the velocity to zero in each point of the field of view (thin lines), a significant anti-

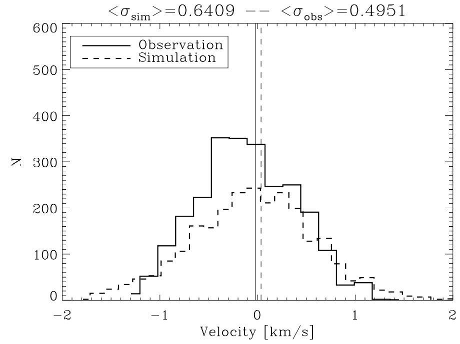

Fig. 5. Velocity histogram obtained for the IBIS observations (solid line) and the synthetic data (dashed line). The vertical lines indicate the mean of the distribution. We also indicate the standard deviation of both distributions, pointing out that the synthetic velocity distribution has a larger dispersion.

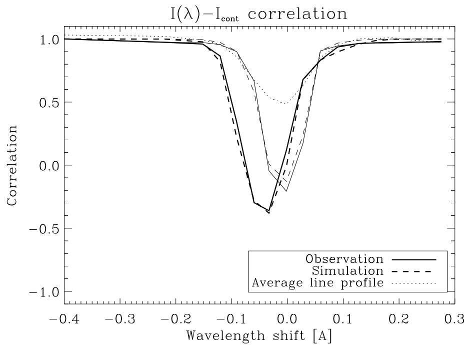

Fig. 4. Correlation between the intensity at each wavelength and the intensity in the continuum for the observations and the synthetic profiles. In thin lines we show the same results but when the velocity of the line at each spatial point is set to zero. The fitting between the synthetic correlation and the observed one is almost perfect.

correlation is obtained only in the core of the line, while both the blue and red wings are directly correlated with the standard granulation. This is an indication that the "formation region" of the core of the Fe I 7090 Å line lies above the zone where the temperature profiles of the granules and intergranules cross. Finally, Figure 5 presents the comparison of the velocity histograms. The velocity at each point has been obtained as the wavelength shift of the core of the line with respect to the core of the spatially averaged spectral line. The vertical lines present the mean value of the distribution, and the simulations correctly recover this value. However, they present points with large velocities, above 1.2 km/s, that are not detected in the observations. This is an issue that will be the subject of further investigation. On the one hand, high velocities in the simulations are necessary to produce the broadening of the average spectral line (Figure 1) without introducing any artificial micro- or macroturbulence parameter. On the other, the high degree of agreement between the observed data and the simulations, as outlined in Figures 3 and 4, seems to indicate that the sign and relative amplitude of the velocities are well recovered in the data. A reduction of the absolute value of the velocities could be due to an actual spatial resolution of the observations still below that adopted for the simulation, or to a selection effect introduced by using only one snapshot out of the whole 2 hours simulations. Our plans in the future are to extend this investigation to other snapshots of the simulation and eventually to the whole time evolution.

Acknowledgements. This research has been funded by the European Commission through the Solar Magnetism Network (ESMN, contract HPRN-CT-2002-00313).

References

Asplund, M., Ludwig, H. G., Nordlund, Å., & Stein, R. F. 2000, A&A, 359, 669

Brault J., Neckel H., 1987, Spectral atlas of solar absolute disk-averaged and disk-center intensity from 3290 to 12510 Å, available at ftp.hs.uni-hamburg.de/pub/outgoing/FTS-atlas

Collados, M., & Vázquez, M. 1987, A&A, 180, 223

Olson, G. L., Auer, L. H., & Buchler, J. R. 1986, J. Quant. Spec. Radiat. Transf., 35, 431